



# Structural and spectroscopic characterization of 2-mesityl-1*H*-benzo[*d*]imidazol-3-ium chloride: A combined experimental and theoretical analysis

Namık Özdemir\*

Department of Physics, Faculty of Arts and Sciences, Ondokuz Mayıs University, 55139 Kurupelit, Samsun, Turkey

## ARTICLE INFO

### Article history:

Received 1 November 2011

Accepted 27 January 2012

### Keywords:

Crystal structure

DFT calculations

IR and NMR spectroscopy

Intermolecular proton transfer

Non-linear optical properties

## ABSTRACT

The title molecular salt, 2-mesityl-1*H*-benzo[*d*]imidazol-3-ium chloride ( $C_{16}H_{17}N_2^+ \cdot Cl^-$ ), was synthesized unexpectedly from the reaction of *N*-[(1*E*)-mesitylmethylene]benzene-1,2-diamine and  $CoCl_2 \cdot 6H_2O$ , and characterized by elemental analysis,  $^1H$  NMR and FT-IR spectroscopies, and single-crystal X-ray diffraction technique. In addition, quantum chemical calculations employing density functional theory (DFT) method with the 6–311++G(d,p) basis set were performed to study the molecular, spectroscopic and some electronic structure properties of the title compound, and the results were compared with the experimental findings. The computational result shows that the optimized geometry can well reproduce the crystal structural parameters. The intermolecular proton transfer process between the ionic ( $C_{16}H_{17}N_2^+ \cdot Cl^-$ ) and nonionic forms ( $C_{16}H_{16}N_2 \cdot HCl$ ) of the title salt is investigated and found to be almost barrierless with an energy value of  $0.20 \text{ kcal mol}^{-1}$ . The NLO properties of the compound are bigger than those of urea.

© 2012 Elsevier B.V. All rights reserved.

## 1. Introduction

Benzimidazoles are regarded as a promising class of bioactive heterocyclic compounds that exhibit a range of biological activities. Because of its synthetic utility and broad range of pharmacological activities, the benzimidazole nucleus is an important heterocyclic ring. Specifically, this nucleus is a constituent of vitamin-B12 [1]. This ring system is present in numerous antioxidant [2–4], antiparasitic [5,6], antihelmintics [7], antiproliferative [8], anti-HIV [9], anticonvulsant [10], antiinflammatory [11,12], antihypertensive [13,14], antineoplastic [15,16], antitrichinellosis [17], antimicrobial [18,19], antihistaminic [20], antifungal [21,22], and anticancer [23] activities. Owing to the immense importance and varied bioactivities exhibited by benzimidazoles, efforts have been made from time to time to generate libraries of these compounds and screened them for potential biological activities.

It is also well known that imidazole-containing molecules can easily coordinate to metal ions as well as act as hydrogen-bond acceptors or donors in supramolecular assembly reactions [24,25], and thus their chemistry has been investigated extensively in coordination chemistry [26,27]. The inclusion of benzimidazole functional group can lead to different coordination modes and may play a crucial role in the construction of supramolecular

compounds driven by hydrogen-bonding interactions [28,29]. In addition, benzimidazole-based organic ligands and their metal complexes continue to attract interest as components in homogeneous catalysis [30]. These different applications have attracted many experimentalists and theorist to investigate the spectroscopic and structural properties of benzimidazole [31–33] and some of its derivatives [34].

Looking at the importance of benzimidazole nucleus, it was thought that it would be worthwhile to design and synthesize some new benzimidazole derivatives. In this study, I present results of a detailed investigation of the synthesis and structural characterization of the title compound using single crystal X-ray diffraction, IR–NMR spectroscopy and quantum chemical methods. The calculations were performed at the DFT/B3LYP level of theory using the 6–311++G(d,p) basis function. These calculations are valuable for providing insight into molecular parameters and the vibrational and NMR spectra. The aim of this work is to explore the molecular dynamics and the structural parameters that govern the chemical behavior, and to compare predictions made from theory with experimental observations.

## 2. Materials and methods

### 2.1. General remarks

All reagents were obtained from commercial suppliers and used without further purification. The elemental analyses were

\* Tel.: +90 362 3121919/5256; fax: +90 362 4576081.

E-mail address: [namiko@omu.edu.tr](mailto:namiko@omu.edu.tr)

determined on a Thermo Finnigan EA 1112 Series Flash Elemental Analyser and Varian SpectrAA 220FS atomic absorption spectrometer. The  $^1\text{H}$  NMR spectra were recorded on a Bruker 300 MHz Ultrashield TM NMR spectrometer in  $\text{CDCl}_3$  with TMS as the internal standard. Melting points were determined in open capillary tubes on an Electrothermal 9100 melting point detection apparatus. Thermal data were obtained by using Perkin-Elmer Diamond Thermal Analysis. The TG-DTA measurements were made between 20 and  $1000^\circ\text{C}$  (in  $\text{N}_2$ ,  $10^\circ\text{C min}^{-1}$ ). The infrared spectra were measured by Perkin-Elmer Spectrum One FT-IR system, and were recorded using universal ATR sampling accessory ( $4000\text{--}550\text{ cm}^{-1}$ ).

## 2.2. Syntheses

### 2.2.1. *N*-[(1*E*)-mesitylmethylene]benzene-1,2-diamine (**1**)

**1** was prepared by a modification of literature method [35]. A mixture of *o*-phenylenediamine (1.1 g, 10 mmol) and 2,4,6-trimethylbenzaldehyde (1.51 ml, 10 mmol) in EtOH (30 ml) was stirred at  $5^\circ\text{C}$  for 2 h. In due course, a yellow suspension was obtained, which was filtered to furnish the product as a yellow solid. Yield: 2.2 g (93%). M.p.:  $120\text{--}122^\circ\text{C}$ . Anal. Calc. for  $\text{C}_{16}\text{H}_{18}\text{N}_2$  (238.33 g): C, 80.63; H, 7.61; N, 11.75. Found: C, 80.66; H, 7.59; N, 11.85%.  $^1\text{H}$  NMR (300 MHz,  $\text{CDCl}_3$ ,  $24^\circ\text{C}$ ): 2.30 (s, 3H), 2.60 (s, 6H), 4.16 (b, 2H), 6.82 (d,  $J = 7.5\text{ Hz}$ , 2H), 6.97 (s, 2H), 7.03–7.13 (m, 2H), 8.95 (s, 1H).

### 2.2.2. 2-Mesityl-1*H*-benzo[d]imidazol-3-ium chloride (**2**)

The title compound (**2**) was isolated by the following procedure (Scheme 1). A solution of  $\text{CoCl}_2 \cdot 6\text{H}_2\text{O}$  (0.1 g, 0.412 mmol) in 20 ml of MeOH was added drop-wise to a solution of **1** (0.196 g, 0.824 mmol) in 20 ml of MeOH. The resulting brown solution was refluxed for 2 h and was concentrated (5 ml).  $\text{Et}_2\text{O}$  was added with stirring to a final volume of 20 ml causing a brown powder to precipitate. The precipitate was filtered off, washed with  $\text{Et}_2\text{O}$ , and dried. X-ray quality crystals were grown from a mixture of MeOH/ $\text{Et}_2\text{O}$ . Yield: 240 mg (68%). M.p.:  $244^\circ\text{C}$  (dec.). Anal. Calc. for  $\text{C}_{16}\text{H}_{17}\text{ClN}_2$  (272.77 g): C, 70.45; H, 6.28; N, 10.27. Found: C, 70.44; H, 6.24; N, 10.45%.  $^1\text{H}$  NMR (300 MHz,  $\text{CDCl}_3$ ,  $24^\circ\text{C}$ ): 1.87 (s, 3H), 2.18 (s, 6H), 6.53–6.79 (b, 4H), 7.11 (s, 2H).

## 2.3. X-ray crystal structure determination

A suitable single crystal of **2** was chosen for the crystallographic study and then carefully mounted on goniometer of a STOE diffractometer with an IPDS II image plate detector. All diffraction measurements were performed at room temperature (296 K) using graphite monochromated Mo  $K\alpha$  radiation ( $\lambda = 0.71073\text{ \AA}$ ) in  $\omega$ -scanning mode. The structure was solved by direct methods using SHELXS-97 [36] implemented in WinGX [37] program suit. All non-hydrogen atoms were refined anisotropically by the full-matrix least squares procedure based on  $F^2$  using SHELXL-97 [38]. All H atoms were positioned geometrically and treated using a riding model, fixing the bond lengths at 0.86, 0.93 and  $0.96\text{ \AA}$  for NH, CH and  $\text{CH}_3$  atoms, respectively. The displacement parameters of the H atoms were fixed at  $U_{\text{iso}}(\text{H}) = 1.2U_{\text{eq}}$  ( $1.5U_{\text{eq}}$  for methyl) of their parent atoms. The H atoms of the methyl group were disordered about a twofold crystallographic axis, and were allowed for by placing six H atoms with equivalent half-occupancies. Data collection: X-AREA [39], cell refinement: X-AREA, data reduction: X-RED32 [39]. Details of the data collection conditions and the parameters of refinement process are given in Table 1. The general-purpose crystallographic tool PLATON [40] was used for the structure analysis and presentation of the results.

**Table 1**  
Crystal data and structure refinement parameters for **2**.

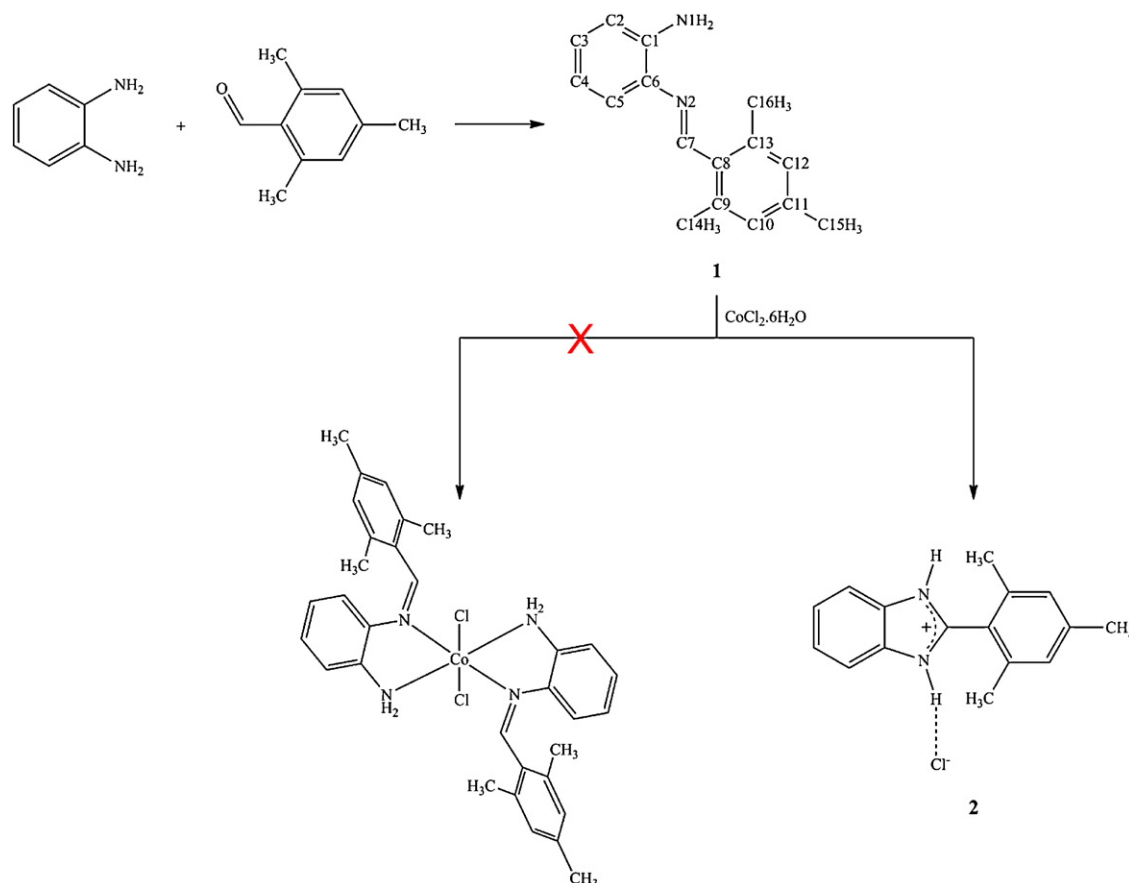
CCDC deposition no.	803481
Color/shape	Brown/leaf like plate
Chemical formula	$\text{C}_{16}\text{H}_{17}\text{N}_2 \cdot \text{Cl}^-$
Formula weight	272.77
Temperature (K)	296
Wavelength ( $\text{\AA}$ )	0.71073 Mo $K\alpha$
Crystal system	Orthorhombic
Space group	$Fddd$ (No. 70)
Unit cell parameters	
$a, b, c$ ( $\text{\AA}$ )	9.4482(6), 13.8602(10), 42.943(3)
Volume ( $\text{\AA}^3$ )	5623.6(7)
$Z$	16
$D_{\text{calc}}$ ( $\text{g/cm}^3$ )	1.289
$\mu$ ( $\text{mm}^{-1}$ )	0.259
Absorption correction	Integration (X-RED32)
$T_{\text{min}}, T_{\text{max}}$	0.8428, 0.9782
$F_{000}$	2304
Crystal size ( $\text{mm}^3$ )	$0.80 \times 0.41 \times 0.06$
Diffractometer/measurement method	STOE IPDS II/rotation ( $\omega$ scan)
Index ranges	$-11 \leq h \leq 11, -17 \leq k \leq 17, -54 \leq l \leq 54$
$\theta$ Range for data collection ( $^\circ$ )	$1.90 \leq \theta \leq 26.81$
Reflections collected	15,097
Independent/observed reflections	1504/1220
$R_{\text{int}}$	0.0587
Refinement method	Full-matrix least-squares on $F^2$
Data/restraints/parameters	1504/0/91
Goodness-of-fit on $F^2$	1.021
Final $R$ indices [ $I > 2\sigma(I)$ ]	$R_1 = 0.0443, wR_2 = 0.1019$
$R$ indices (all data)	$R_1 = 0.0628, wR_2 = 0.1105$
$\Delta\rho_{\text{max}}, \Delta\rho_{\text{min}}$ ( $\text{e/\AA}^3$ )	0.16, $-0.27$

## 2.4. Computational details

All geometries were fully optimized in the ground state using the Berny algorithm [41] without symmetry restrictions and using the default convergence criteria. The cartesian coordinates of the X-ray structure were used as the starting geometry for the theoretical calculations. The calculations were performed by means of the Gauss View molecular visualization program [42] and Gaussian 03 program package [43] using the spin-restricted hybrid density functional theory (B3LYP) [44,45] method with the 6-311++G(d,p) [46,47] basis set. A scale factor of 0.9668 [48] was used to correct the calculated vibrational frequencies. The  $^1\text{H}$  NMR chemical shifts were calculated within the gauge-independent atomic orbital (GIAO) approach [49,50] applying the same method and the basis set as used for geometry optimization. The  $^1\text{H}$  NMR chemical shifts were converted to the TMS scale by subtracting the calculated absolute chemical shielding of TMS ( $\delta = \Sigma_0 - \Sigma$ , where  $\delta$  is the chemical shift,  $\Sigma$  is the absolute shielding and  $\Sigma_0$  is the absolute shielding of TMS), whose value is 31.96 ppm. The effect of solvent on the theoretical NMR parameters was included using the default model IEF-PCM (Integral-Equation-Formalism Polarizable Continuum Model) [51] provided by Gaussian 03. Chloroform was used as solvent. All the geometry optimizations were followed by frequency calculations and no imaginary frequencies were found. That is to say, the structures obtained from geometry optimization correspond to stationary points in the potential surfaces and they are stationary structures.

## 3. Results and discussion

Compound **1** was obtained from *o*-phenylenediamine and 2,4,6-trimethylbenzaldehyde. However, compound **2** occurred unexpectedly from the reaction of compound **1** and  $\text{CoCl}_2 \cdot 6\text{H}_2\text{O}$  in 1:1 molar ratio, while I plan to synthesize the cobalt(II) complex (see Scheme 1). The elemental analysis and atomic absorption



**Scheme 1.** The formation of **2**.

spectrometer results of the compound being formed suggest the formula  $C_{16}H_{17}ClN_2$ . The TG-DTA curves of compound **2** show that the compound starts decomposition at  $244^\circ\text{C}$  (see Fig. S1 in the supplementary material).

### 3.1. Crystallographic results

The title compound (**2**), a DIAMOND [52] view of which is shown in Fig. 1, is a salt crystallizing in the orthorhombic space group  $Fddd$  with  $Z = 16$ , and composed of a 2-mesityl-1H-benzo[d]imidazol-3-ium cation and one chloride anion. Both ions are located on special positions, allowing them to straddle a twofold rotation axis along [001], so that the asymmetric unit contains the anion and one-half of the cation. The twofold rotation axis bisects the benzimidazole and mesityl rings, passing through C1, C5, C8 and C10 atoms. As a result, the methyl group on the twofold axis is disordered.

The benzimidazole and benzene rings of the molecule are not coplanar but rather have a dihedral angle of  $56.78(8)^\circ$ ; the N1–C1–C5–C6<sup>i</sup> torsion angle is  $-55.80(11)^\circ$ . Furthermore, the dihedral angle between the five- and six-membered rings of the benzimidazole ring system is  $1.34(14)^\circ$ , and the maximum deviation from planarity is  $0.0206(14)$  Å for atom N1, while the crossed torsion angles at the junction, i.e. N1–C2–C2<sup>i</sup>–C3<sup>i</sup> and N1<sup>i</sup>–C2<sup>i</sup>–C2–C3, are both equal to  $-178.24(15)^\circ$ .

The N1–C1 and N1–C2 bond lengths in the imidazole ring are significantly different, being  $1.341(2)$  and  $1.389(2)$  Å, respectively. These distances are comparable with the average values found for 2-amino-1H-benzo[d]imidazolium squarate [ $1.339$  and  $1.391$  Å, respectively; [53]], 2-(2-acetamido-4-methylthiazol-5-yl)-1H-benzo[d]imidazol-3-ium chloride tetrahydrate [ $1.340$  and  $1.387$  Å, respectively; [54]], 2-amino-1H-benzo[d]imidazol-3-ium

phthalate [ $1.339$  and  $1.394$  Å, respectively; [55]] and 2-amino-6-nitro-1H-benzoimidazol-3-ium chloride [ $1.340$  and  $1.387$  Å, respectively; [56]].

The N1–C1 and N1<sup>i</sup>–C1 bond distances are equal to each other, and show an intermediate character between single and double bonds [57], indicating dispersion of positive charge over both N atoms in the imidazole ring. In addition, a survey of the Cambridge Structural Database (CSD, Version 5.31) [58] for only organic compounds, which has been searched using ConQuest software (Version 1.12) [59], revealed that the N1–C1–N1<sup>i</sup> angle [ $107.7(2)^\circ$ ] in the title compound has decreased when compared to those of the non-protonated benzimidazoles groups [ $109.751$ – $114.569^\circ$ ].

The molecular structure does not exhibit any intramolecular hydrogen bonds. In the crystal structure, the benzimidazole cation is connected to the anion by means of N–H...Cl hydrogen bond, therefore, the C–N bonds mentioned above have intermediate values between the expected single and double bond lengths. Propagation of this hydrogen-bonding motif then generates a chain of molecules running approximately along the [110] and  $[\bar{1}10]$  directions (Fig. 2). The full geometry of this intermolecular interaction is given in Table 2. There are no other significant intermolecular interactions in the crystal structure of **2**.

### 3.2. Spectroscopic characterization

#### 3.2.1. IR spectroscopy

The FT-IR spectra of compounds **1** and **2** are presented in Figs. 3 and 4, respectively, while the main vibrational bands are given in Table 3. In the IR spectrum of **1**, the  $\nu(\text{C}=\text{O})$  stretching band in the range of  $1700$ – $1750\text{ cm}^{-1}$  disappears due to the formation of a C=N bond between the amine and the aldehyde group,

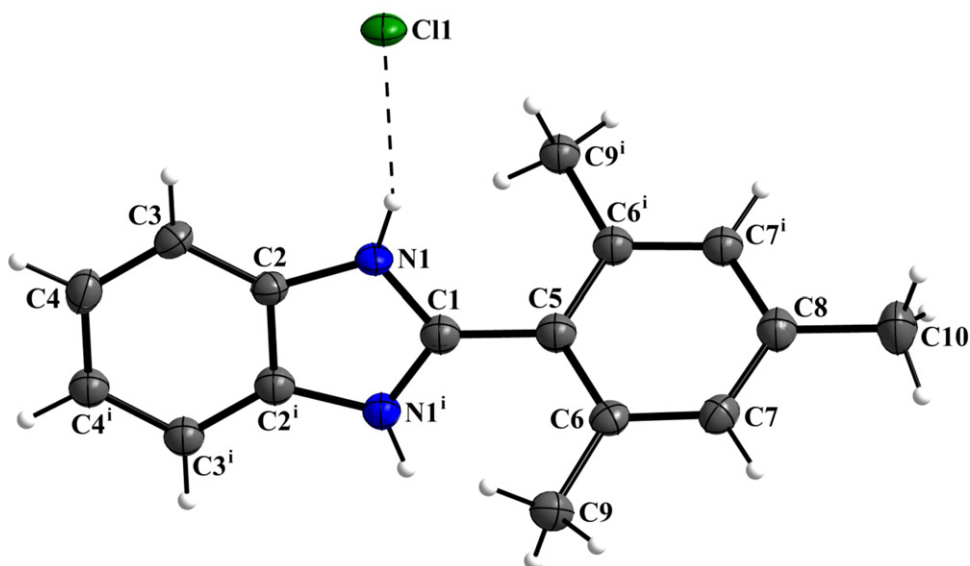


**Fig. 1.** The molecular structure of **2** showing the atom-numbering scheme. Displacement ellipsoids are drawn at the 30% probability level and H atoms are shown as small spheres of arbitrary radii. The dashed lines represent the Cl...H contact. Only one orientation of the disordered methyl group is shown. (Symmetry code:  $i = -x + 3/4, -y + 3/4, z$ ).

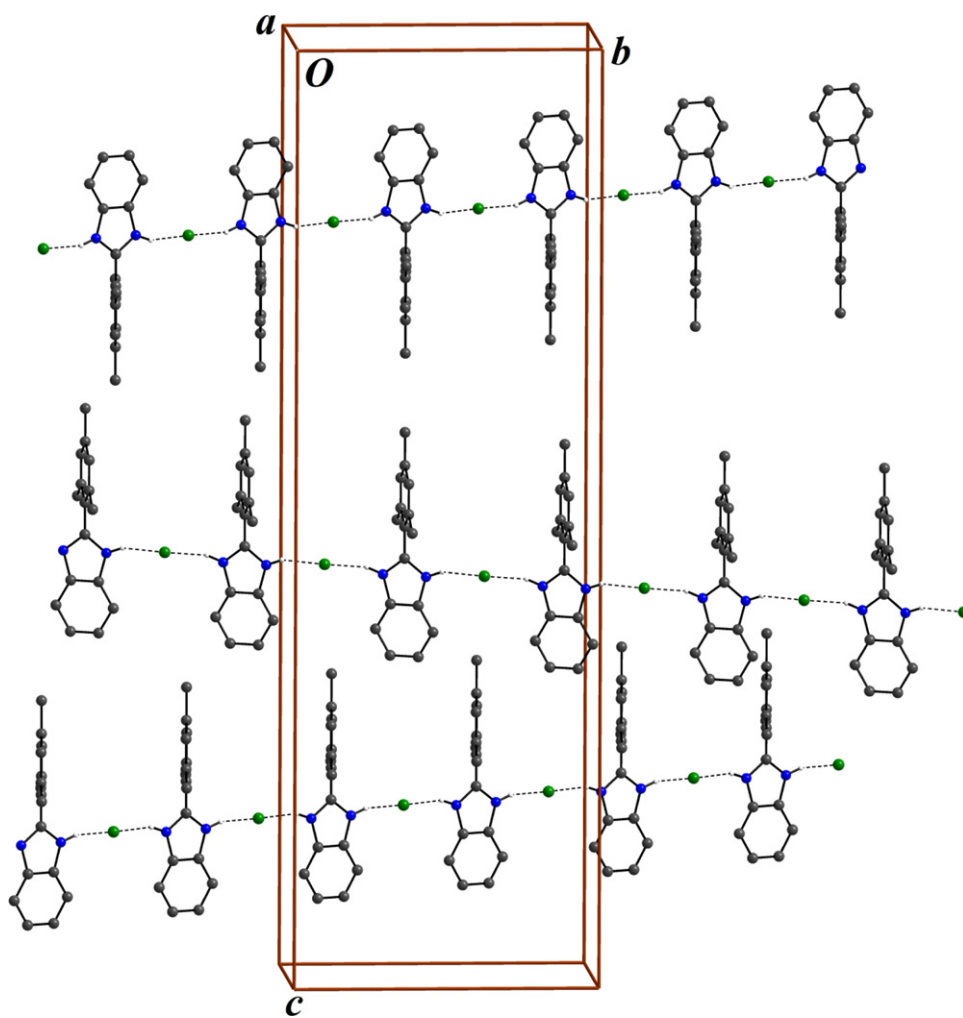


**Fig. 2.** Part of the crystal structure of **2**, showing the formation of one-dimensional linear chains of molecules along  $[110]$  and  $[\bar{1}10]$ . For the sake of clarity, H atoms not involved in the motif shown have been omitted.

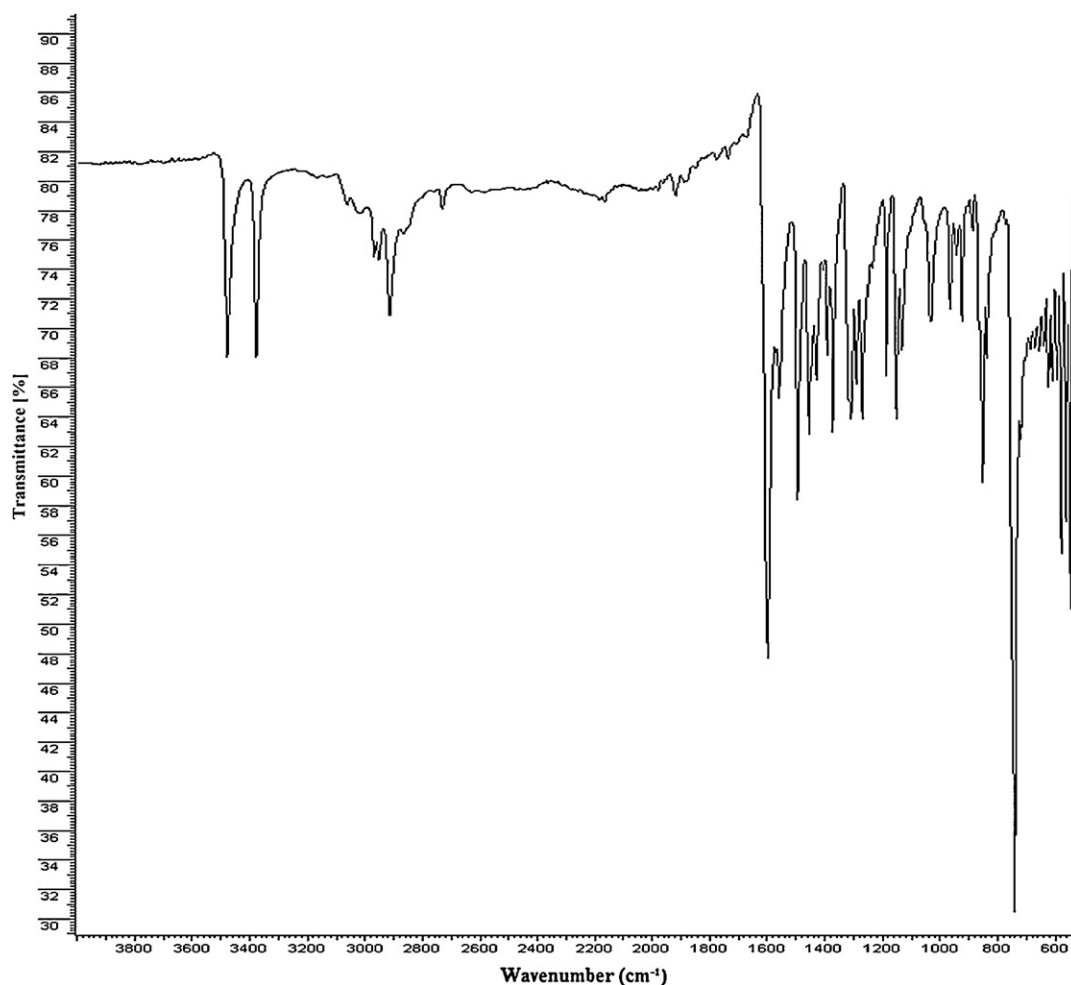


Fig. 3. FT-IR spectrum of **1**.

while the  $\nu(\text{C}=\text{N})$  stretching vibration is observed at  $1598\text{ cm}^{-1}$ . This band has been calculated at  $1612\text{ cm}^{-1}$ . The stretching, in-plane and out-of-plane bending bands assigned to the methine group are monitored at  $2951$ ,  $1372$  and  $965\text{ cm}^{-1}$ , which have been appeared in  $2947$ ,  $1378$  and  $964\text{ cm}^{-1}$  in the theoretical spectra. The asymmetric and symmetric  $\nu(\text{N}-\text{H}_2)$  stretching bands are observed at  $3478$  and  $3377\text{ cm}^{-1}$ , that have been calculated at  $3540$  and  $3431\text{ cm}^{-1}$ , respectively.

The solid phase of the compound includes various crystal interactions. Benzimidazole derivatives are known to be strongly associated through intermolecular hydrogen bonding. In the IR spectrum of **2**, the stretching band assigned to  $\nu(\text{N}-\text{H})$  is monitored at  $3551\text{ cm}^{-1}$ , which is found to be  $3530\text{ cm}^{-1}$  theoretically. The region at  $1660\text{--}1480\text{ cm}^{-1}$  is very characteristic of benzimidazoles [60], in which the  $\nu(\text{C}=\text{N})$  and  $\nu(\text{C}=\text{C})$  stretching vibrations were observed. The band observed at  $1609\text{ cm}^{-1}$  is attributed to the  $\nu(\text{C}=\text{N})$  vibration, while the bands observed at  $1574$  and  $1554\text{ cm}^{-1}$  can be attributed to the  $\text{C}=\text{C}$  stretching vibrations. These bands have been calculated at  $1608$ ,  $1590$  and  $1552\text{ cm}^{-1}$ , respectively. All these data also agree with the results of the study of Sundaraganesan et al. [61].

Table 2  
Hydrogen bonding geometry for **2**.

D-H...A	D-H (Å)	H...A (Å)	D...A (Å)	D-H...A (°)
N1-H1...C11	0.86	2.31	3.1254(13)	159

To make a comparison with experimental observations, I studied the correlation between the calculated and the experimental data, and obtained correlation coefficients of 0.99969 and 0.9997 for compounds **1** and **2**, respectively. These results show that there is a good correlation between the theoretical and experimental vibrational frequencies.

### 3.2.2. NMR spectroscopy

The characterization of the compound was further enhanced by the use of  $^1\text{H}$  NMR spectroscopy. The  $^1\text{H}$  NMR spectra of compounds **1** and **2** are shown in Figs. 5 and 6. In addition, theoretical  $^1\text{H}$  NMR chemical shift values of the compounds have been computed using the same method and the basis sets for the two optimized geometries. The results of these calculations are tabulated in Table 4 together with the experimental values. Since experimental  $^1\text{H}$  chemical shift values were not available for individual hydrogen atoms of  $\text{NH}_2$  and  $\text{CH}_3$  groups, I have presented the average of the computed values for these hydrogen atoms.

The  $^1\text{H}$  NMR spectrum of **1** shows two singlet signals assigned to the  $\text{CH}_3$  protons at 2.30 (3H) and 2.60 (6H) ppm because of different chemical environments, which have been computed as average values of 2.42 and 2.62–2.75 ppm, respectively. These signals are shifted upfield by 1.87 and 2.18 ppm in the spectrum of **2**, while the theoretical average value for these protons is determined as 2.50 and 2.27–2.62 ppm, respectively. The signals assigned to the phenyl protons at the range 6.82–7.13 ppm in the spectrum of **1** are shifted low frequencies in the spectrum of **2**. When the  $^1\text{H}$  NMR

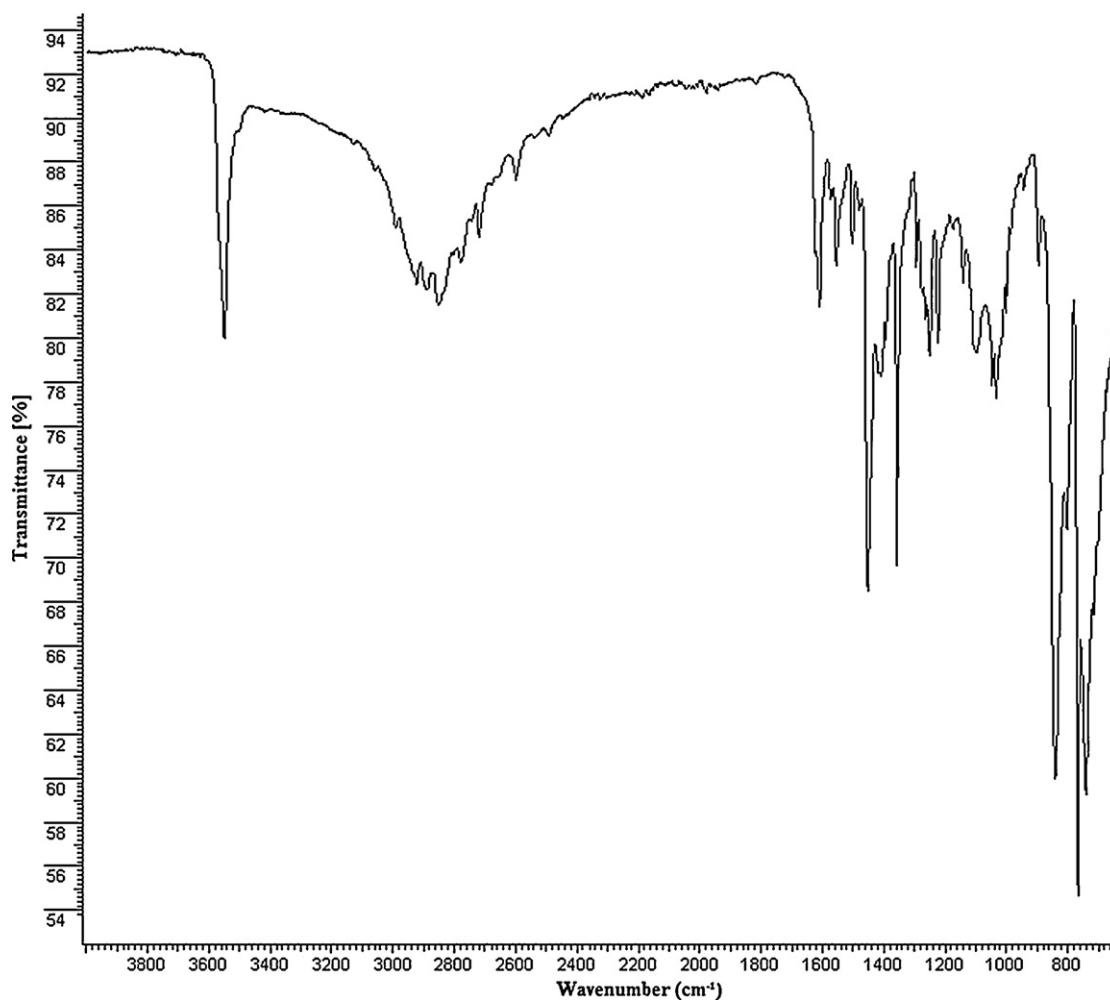


Fig. 4. FT-IR spectrum of **2**.

spectrum of **2** was compared to that of **1**, the signals attributed to the  $\text{NH}_2$  and  $\text{CH}=\text{N}$  did not appear in the  $^1\text{H}$  NMR spectrum of **2**. This approves that the expected Co(II) complex compound did not form as supported by the elemental analysis and atomic absorption spectrometer results.

### 3.3. Quantum-chemical studies

#### 3.3.1. Theoretical structure

The molecular structure of title compound was also studied theoretically. The starting coordinates were those obtained from the X-ray structure determination and were optimized by energy-minimization with the density functional theory (DFT) method. Some selected geometrical parameters experimentally obtained and theoretically calculated are listed in Table 5.

As can be seen in Table 5, agreement between the calculated structure and the experimentally determined X-ray crystal structure is satisfactory. However, when the X-ray structure of the title compound is compared with its optimized counterpart (see Fig. 7), some conformational discrepancies are observed between them. The dihedral angle between the benzimidazole and benzene rings of the title molecule is calculated at  $61.606^\circ$ , while the dihedral angle between the five- and six-membered rings of the benzimidazole ring system is computed at  $0.022^\circ$ .

A logical method for globally comparing the structure obtained with the theoretical calculation is by superimposing the molecular

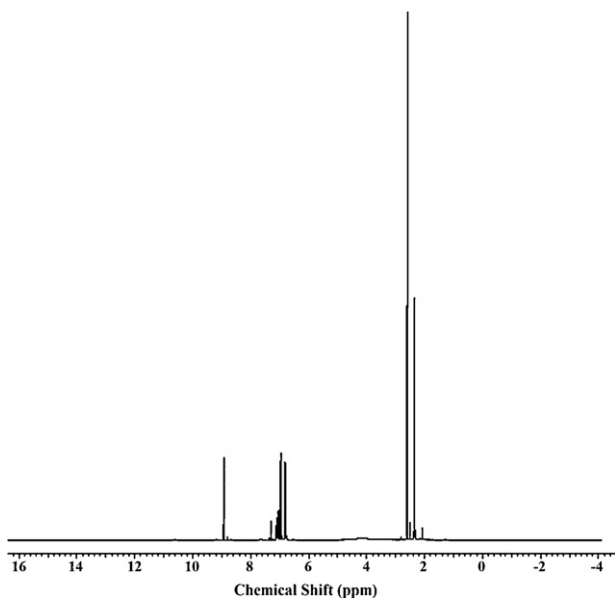


Fig. 5. 300 MHz  $^1\text{H}$  NMR spectrum of **1** in  $\text{CDCl}_3$ .

**Table 3**  
Comparison of the observed and calculated vibrational spectra of compounds **1** and **2**.

Assignments	<b>1</b>		<b>2</b>	
	Exp. (cm <sup>-1</sup> )	Calc. (cm <sup>-1</sup> )	Exp. (cm <sup>-1</sup> )	Calc. (cm <sup>-1</sup> )
$\nu$ N–H	–	–	3551	3530
$\nu_{as}$ N–H <sub>2</sub>	3478	3540	–	–
$\nu_s$ N–H <sub>2</sub>	3377	3431	–	–
$\nu_s$ C–H (Ar)	3063	3084	3132	3102
$\nu_{as}$ C–H (Ar)	3020	3050	3058	3071
$\nu_{as}$ C–H <sub>3</sub>	3002	3002	2990	3005
$\nu_{as}$ C–H <sub>3</sub>	2968	2973	–	–
$\nu$ C–H (Mt)	2951	2947	–	–
$\nu_s$ C–H <sub>3</sub>	2913	2920	2889	2917
$\nu$ C=N	1598	1612	1609	1608
$\nu$ C=C	–	–	1574	1590
$\alpha$ N–H <sub>2</sub>	1558	1584	–	–
$\nu$ C=C	1494	1538	1554	1552
$\nu$ C–C(NH) <sub>2</sub> + $\gamma$ N–H	–	–	1502	1542
$\gamma$ N–H + $\gamma$ C–H	–	–	1479	1484
$\alpha$ C–H <sub>3</sub>	1456	1463	1451	1467
$\gamma$ N–H + $\gamma$ C–H	–	–	1413	1427
$\alpha$ C–H <sub>3</sub>	1429	1427	1393	1394
$\gamma$ C–H (Mt)	1372	1378	–	–
$\omega$ C–H <sub>3</sub>	1317	1366	1356	1367
$\gamma$ N–H + $\gamma$ C–H	–	–	1293	1311
$\nu$ C=C + $\gamma$ C–H (Ar)	1309	1309	1262	1258
$\nu$ C–NH <sub>2</sub>	1291	1286	–	–
$\nu$ C=C + $\gamma$ C–H (Ar)	1270	1274	–	–
$\gamma$ N–H + $\gamma$ C–H	–	–	1222	1233
$\nu$ C–N + $\gamma$ C–H (Ar)	1153	1171	–	–
$\gamma$ C–H (Ar)	1133	1142	1141	1136
$\omega$ N–H	–	–	1046	1061
$\gamma$ N–H <sub>2</sub> + $\gamma$ C–H (Ar)	1031	1046	–	–
$\delta$ C–H <sub>3</sub>	–	–	1025	1029
$\gamma$ C–H	–	–	985	993
$\omega$ C–H (Mt)	965	964	–	–
$\delta$ C–H (Ar)	838	839	841	838
$\theta$	740	756	766	786
$\omega$ C–H (Ar)	720	726	740	745
$\omega$ C–H	–	–	715	730
$\omega$ N–H <sub>2</sub>	577	592	–	–
$\theta$	547	553	–	–
$\beta$ ring def	531	540	–	–

Vibrational modes:  $\nu$ , stretching;  $\alpha$ , scissoring;  $\gamma$ , rocking;  $\omega$ , wagging;  $\delta$ , twisting;  $\theta$ , ring breathing. Abbreviations: as, asymmetric; s, symmetric; Ar, aromatic; Mt, methine.

skeleton with that obtained from X-ray diffraction, giving an RMSE of 0.052 Å (Fig. 7). This value shows that there is a good correlation between the experimental and calculated structures. However, it was noted here that the experimental results belong to solid phase and theoretical calculations belong to gaseous phase. In the solid state, the existence of the crystal field along with the intermolecular interactions has connected the molecules together, which result in the differences of bond parameters between the calculated and experimental values.

**Table 4**  
Experimental and theoretical <sup>1</sup>H NMR chemical shifts  $\delta$ (ppm) from TMS for compounds **1** and **2**.

<b>1</b>			<b>2</b>		
Atom	Experimental	Calculated	Atom	Experimental	Calculated
H1	4.16 (b, 2H)	4.32 <sup>a</sup>	H1	–	22.04
H2, H5	7.03–7.13 (m, 2H)	7.12	H1 <sup>i</sup>	–	8.71
H3, H4	6.82 (d, $J=7.5$ Hz, 2H)	6.96–7.45	H3, H3 <sup>i</sup> , H4, H4 <sup>i</sup>	6.53–6.79 (b, 4H)	7.69–8.44
H7	8.95 (s, 1H)	9.26	H7, H7 <sup>i</sup>	7.11 (s, 2H)	7.35–7.37
H10, H12	6.97 (s, 2H)	7.27–7.38	H9, H9 <sup>i</sup>	2.18 (s, 6H)	2.27 <sup>a</sup> –2.62 <sup>a</sup>
H14, H16	2.60 (s, 6H)	2.62 <sup>a</sup> –2.75 <sup>a</sup>	H10	1.87 (s, 3H)	2.50 <sup>a</sup>
H15	2.30 (s, 3H)	2.42 <sup>a</sup>			

<sup>a</sup> Average.

Note: The atom numbering according to Scheme 1 used in the assignment of chemical shifts of **1**.

Note: The atom numbering according to Fig. 1 used in the assignment of chemical shifts of **2**.

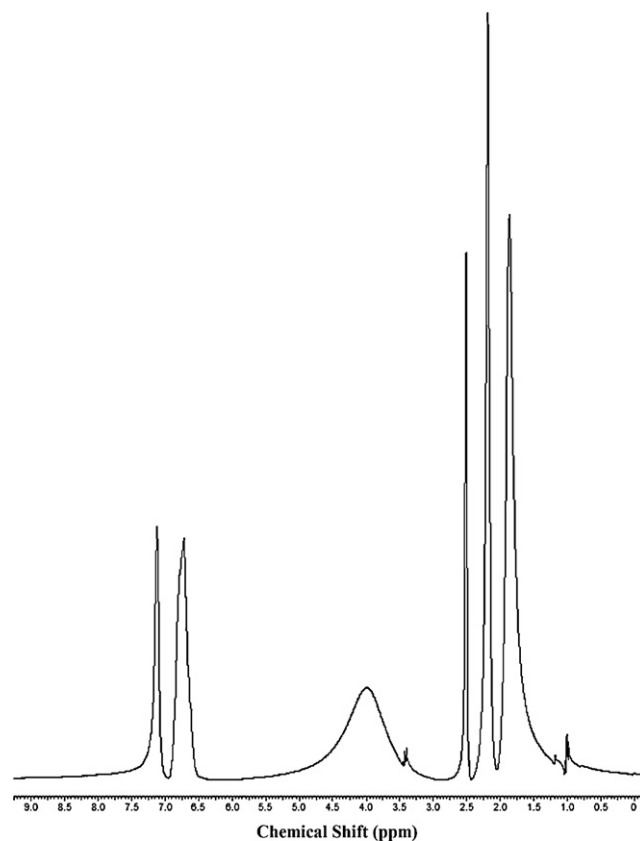


**Fig. 6.** 300 MHz <sup>1</sup>H NMR spectrum of **2** in CDCl<sub>3</sub>.

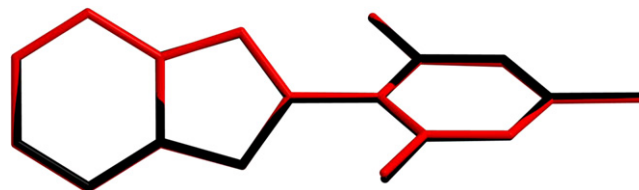


**Fig. 7.** Atom-by-atom superimposition of the X-ray structure (black) of the title compound and its DFT (red) optimized counterpart. Chloride anion and hydrogen atoms omitted for clarity. (For interpretation of the references to color cited in the figure legend, the reader is referred to the web version of the article.)

### 3.3.2. Intermolecular proton transfer

The ionic (I), nonionic (II) and transition state (TS) geometries of the title compound optimized at the B3LYP/6–311++G(d,p) level are shown in Fig. 8, while selected structural parameters are listed in Table 5.

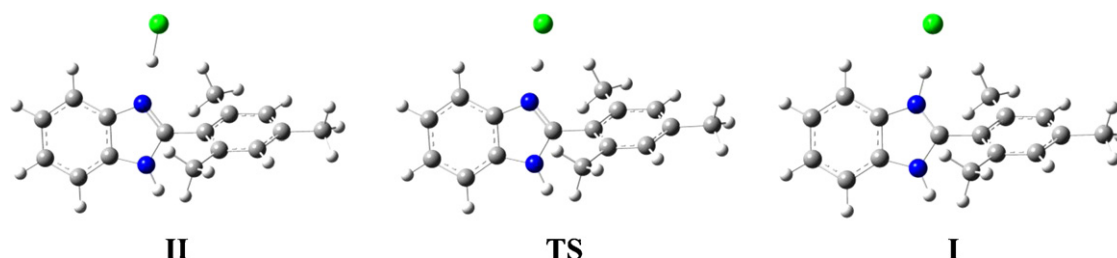


Fig. 8. Optimized molecular structures of the ionic (I), nonionic (II) and transition state (TS) geometries of **2**.

Here, the intermolecular proton transfer reaction  $\text{II} \rightarrow \text{TS} \rightarrow \text{I}$  was examined in the gas phase. Due to the migration of a hydrogen atom from atom N1 to atom C1, some changes are observed in the structure. The distance between atoms C1 and H1 decreases upon the proton transfer  $\text{II} \rightarrow \text{TS} \rightarrow \text{I}$ . The N1–H1 and C1–H1 distances are found to be 1.360 Å and 1.494 Å for TS, respectively. It can be concluded that the N1–H1 bond is broken, and a C1–H1 bond (ca. 1.380 Å) is formed during the intermolecular proton transfer process in the compound. As can be seen from Table 5, in the proton transfer  $\text{II} \rightarrow \text{TS} \rightarrow \text{I}$ , very slight changes are observed in the bond distances of the benzimidazole ring system. However, the N1–C1–N1<sup>i</sup> and N1–C2–C2<sup>i</sup> angles contract as C1–N1–C2 angle expands, approximately 2°. In addition, the dihedral angle between the benzimidazole and benzene rings is reduced from 68.279° to 61.606°.

The tautomerization energy was calculated as the energy differences between the tautomers and the transition state. The energy difference between the two tautomers (I and II) was calculated as  $-0.13 \text{ kcal mol}^{-1}$ . So, it can be said that tautomer I is more stable than tautomer II, but very little energy difference exists between them. The relative energy of the TS with respect to tautomer II was calculated to be  $0.20 \text{ kcal mol}^{-1}$ . As a result, very low barrier height was found for this intermolecular proton transfer reaction.

Table 5  
Optimized and experimental geometries of **2** in the ground state.

Parameters	Experimental	Calculated		
		I	TS	II
Bond lengths (Å)				
C1–H1	–	–	–	1.37946
N1–C1	1.341(2)	1.32481	1.32042	1.31744
N1 <sup>i</sup> –C1	1.341(2)	1.36358	1.36917	1.37383
N1–C2	1.389(2)	1.38661	1.38775	1.38862
N1 <sup>i</sup> –C2 <sup>i</sup>	1.389(2)	1.38991	1.38741	1.38560
N1–H1	0.86	1.16483	–	–
N1 <sup>i</sup> –H1 <sup>i</sup>	0.86	1.00806	1.00790	1.00770
C1–C5	1.458(3)	1.47363	1.47756	1.48009
C2–C2 <sup>i</sup>	1.394(3)	1.40511	1.40775	1.40983
Bond angles (°)				
N1–C1–N1 <sup>i</sup>	107.7(2)	108.98595	110.13018	110.96735
N1–C1–C5	126.15(11)	127.09016	126.87332	126.67276
N1 <sup>i</sup> –C1–C5	126.15(11)	123.92359	122.99625	122.35970
N1–C2–C2 <sup>i</sup>	106.11(8)	107.73061	108.58430	109.22947
N1 <sup>i</sup> –C2 <sup>i</sup> –C2	106.11(8)	105.05774	104.82278	104.64727
N1–C2–C3	132.26(15)	130.85025	130.59522	130.38431
N1 <sup>i</sup> –C2 <sup>i</sup> –C3 <sup>i</sup>	132.26(15)	133.03278	133.02972	133.04019
C1–N1–C2	110.04(14)	108.92704	107.74765	106.87243
C1–N1 <sup>i</sup> –C2 <sup>i</sup>	110.04(14)	109.29822	108.71495	108.28336
Torsion angles (°)				
N1–C1–C5–C6	124.20(11)	118.47229	114.57677	111.80344
N1 <sup>i</sup> –C1–C5–C6 <sup>i</sup>	124.20(11)	118.51635	114.59789	111.91596
N1–C1–C5–C6 <sup>i</sup>	–55.80(11)	–61.26036	–65.20502	–67.91335
N1 <sup>i</sup> –C1–C5–C6	–55.80(11)	–61.75101	–65.62032	–68.36725

<sup>i</sup>–x+3/4, –y+3/4, z.

### 3.3.3. Molecular electrostatic potential

The molecular electrostatic potential,  $V(\mathbf{r})$ , at a given point  $\mathbf{r}(x, y, z)$  in the vicinity of a molecule, is defined in terms of the interaction energy between the electrical charge generated from the molecule electrons and nuclei and a positive test charge (a proton) located at  $\mathbf{r}$ . For the system studied, the  $V(\mathbf{r})$  values were calculated as described previously using the equation [62],

$$V(\mathbf{r}) = \sum_A \frac{Z_A}{|\mathbf{R}_A - \mathbf{r}|} - \int \frac{\rho(\mathbf{r}')}{|\mathbf{r}' - \mathbf{r}|} d\mathbf{r}'$$

where  $Z_A$  is the charge of nucleus  $A$  located at  $\mathbf{R}_A$ ,  $\rho(\mathbf{r}')$  is the electronic density function of the molecule, and  $\mathbf{r}'$  is the dummy integration variable.

The molecular electrostatic potential (MEP) is related to the electronic density and is a very useful descriptor in understanding sites for electrophilic attack and nucleophilic reactions as well as hydrogen-bonding interactions [63,64]. The electrostatic potential  $V(\mathbf{r})$  is also well suited for analyzing processes based on the “recognition” of one molecule by another, as in drug–receptor, and enzyme–substrate interactions, because it is through their potentials that the two species first “see” each other [65]. Being a real physical property,  $V(\mathbf{r})$  can be determined experimentally by diffraction or by computational methods [66].

To predict reactive sites for electrophilic and nucleophilic attack for the title molecule, MEP was calculated by applying the same method and the basis sets as used for geometry optimization. The negative (red color) regions of MEP were related to electrophilic reactivity and the positive (blue color) ones to nucleophilic reactivity shown in Fig. 9. As can be seen from the figure, there is one

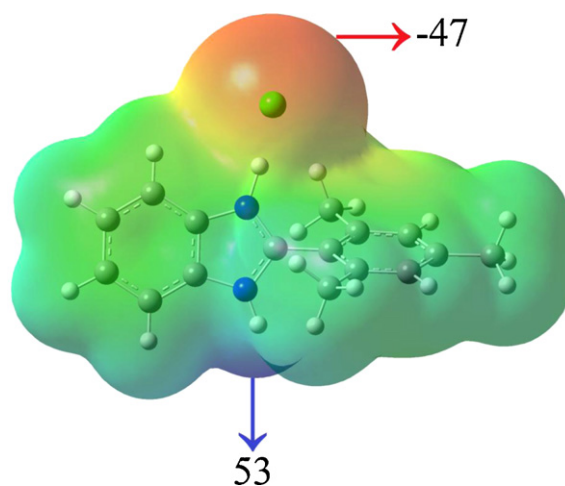
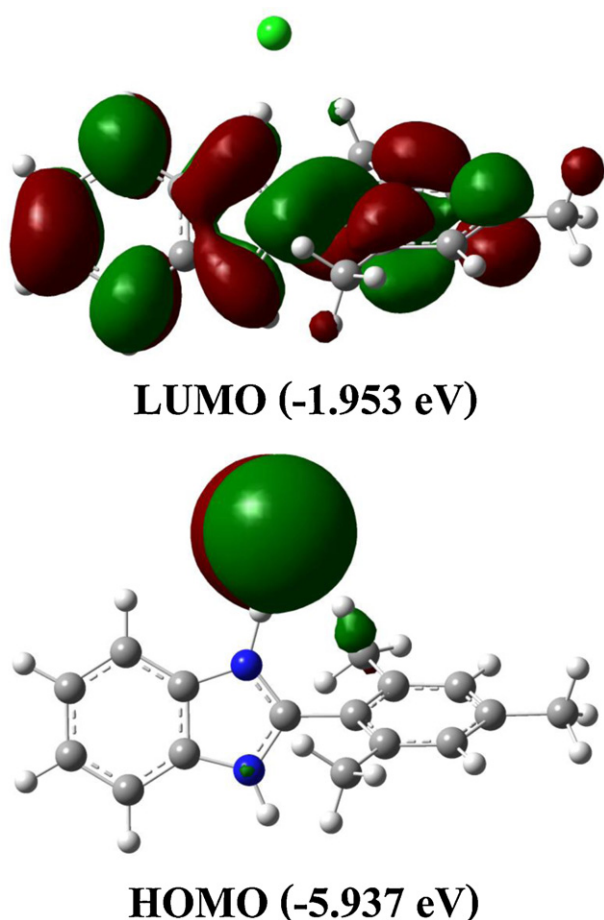


Fig. 9. Molecular electrostatic potential map (in  $\text{kcal mol}^{-1}$ ) of **2** with an isodensity value of  $0.25 \text{ kcal mol}^{-1}$ . (For interpretation of the references to color cited in the text, the reader is referred to the web version of the article.)



**Fig. 10.** Molecular orbital surfaces for the HOMO and LUMO of **2**. The positive phase is red, and the negative phase is green. (For interpretation of the references to color cited in the figure legend, the reader is referred to the web version of the article.)

possible site on the compound for electrophilic attack. The negative region is mainly localized on the chloride anion, Cl1, with a maximum value of  $-47 \text{ kcal mol}^{-1}$ . However, a maximum positive region is mainly over the benzimidazole nitrogen atom, N1, with a maximum value of  $53 \text{ kcal mol}^{-1}$ . So, Fig. 9 confirms the existence of intermolecular N–H...Cl interactions observed in the solid state.

### 3.3.4. Frontier molecular orbitals

The frontier molecular orbitals play an important role in the electric and optical properties, as well as in UV–vis spectra. It is well known that both the highest occupied molecular orbital (HOMO) and lowest unoccupied molecular orbital (LUMO) are the main orbital taking part in chemical reaction. The HOMO energy characterizes the ability of electron giving, LUMO energy characterizes the ability of electron accepting, and the gap between HOMO and LUMO characterizes the molecular chemical stability [67]. Fig. 10 shows the distributions and energy levels of the HOMO–LUMO orbitals computed at the same level as used for geometry optimization for the title compound.

The calculations indicate that the compound has 72 occupied molecular orbitals. As can be seen from the figure, the HOMO and LUMO orbitals are localized on different parts of **2**. The HOMO orbitals are localized on the chloride anion, while the LUMO orbitals are spread over the whole cation molecule. But, both of the highest occupied molecular orbital (HOMO) and the lowest unoccupied molecular orbital (LUMO) are mostly  $\pi$ -antibonding type orbitals. The value of the energy separation between the HOMO and LUMO is

$3.984 \text{ eV}$  and this large energy gap indicates that the title structure is quite stable.

### 3.3.5. Non-linear optical effects

Non-linear optical (NLO) effects arise from the interactions of electromagnetic fields in various media to produce new fields altered in phase, frequency, amplitude or other propagation characteristics from the incident fields [68]. NLO is at the forefront of current research because of its importance in providing the key functions of frequency shifting, optical modulation, optical switching, optical logic, and optical memory for the emerging technologies in areas such as telecommunications, signal processing, and optical interconnections [69,70].

The calculations of the mean linear polarizability ( $\alpha_{tot}$ ) and the mean first hyperpolarizability ( $\beta_{tot}$ ) from the Gaussian output have been explained in detail previously [71]. The total molecular dipole moment ( $\mu_{tot}$ ), linear polarizability ( $\alpha_{tot}$ ) and first-order hyperpolarizability ( $\beta_{tot}$ ) of the title compound were calculated at the B3LYP/6–311++G(d,p) level. The calculated values of  $\mu_{tot}$ ,  $\alpha_{tot}$  and  $\beta_{tot}$  are  $10.735 \text{ D}$ ,  $34.162 \text{ \AA}^3$  and  $5.379 \times 10^{-30} \text{ cm}^5/\text{esu}$ . Urea is one of the prototypical molecules used in the study of the NLO properties of molecular systems. Therefore it was used frequently as a threshold value for comparative purposes. The values of  $\mu_{tot}$ ,  $\alpha_{tot}$  and  $\beta_{tot}$  of urea are  $3.874 \text{ D}$ ,  $5.042 \text{ \AA}^3$  and  $0.765 \times 10^{-30} \text{ cm}^5/\text{esu}$  obtained at the same level. Theoretically, the first-order hyperpolarizability of the title compound is of ca. 7 times magnitude of urea. According to these results, the title compound is a good candidate of NLO material.

## 4. Conclusions

In this paper, I have reported the synthesis and characterization of a novel benzimidazole salt compound (**2**) occurred unexpectedly, together with the results of its electronic structure investigation at the B3LYP/6–311++G(d,p) level. The major conclusions to be gleaned from this work are the following:

1. The structure of **2** is verified by FT-IR,  $^1\text{H}$  NMR, elemental analysis and single crystal X-ray diffraction, as well as by atomic absorption spectroscopy.
2. The structural parameters of the title molecule calculated in the gas phase are in very good correspondence with X-ray experimental data.
3. In the gas phase, the ionic form (I) of **2** is more stable than the nonionic form (II), and very low barrier energy ( $0.20 \text{ kcal mol}^{-1}$ ) is found for the intermolecular proton transfer reaction between them.
4. The MEP map agrees well with the solid state interaction, and a large HOMO–LUMO gap indicates a quite stable structure.
5. The predicted NLO properties of **2** are greater than ones of urea. So, the title compound is a good candidate as second-order NLO material.

## Supplementary material

CCDC 803481 contains the supplementary crystallographic data (excluding structure factors) for the structure reported in this article. These data can be obtained free of charge at [www.ccdc.cam.ac.uk/conts/retrieving.html](http://www.ccdc.cam.ac.uk/conts/retrieving.html) [or from the Cambridge Crystallographic Data Centre (CCDC), 12 Union Road, Cambridge CB2 1EZ, UK. Fax: +44 0 1223 336033; e-mail: [deposit@ccdc.cam.ac.uk](mailto:deposit@ccdc.cam.ac.uk)]

## Acknowledgments

I wish to thank Prof. Dr. Orhan Büyükgüngör for his help with the data collection and acknowledge the Faculty of Arts and Sciences, Ondokuz Mayıs University, Turkey, for the use of the STOE IPDS II diffractometer (purchased under grant No. F-279 of the University Research Fund).

## Appendix A. Supplementary data

Supplementary data associated with this article can be found, in the online version, at [doi:10.1016/j.saa.2012.01.069](https://doi.org/10.1016/j.saa.2012.01.069).

## References

- [1] M.J. O'Neil, M. Smith, P.E. Heckelman, The Merck Index, 13th ed., Merck & Co. Inc., New Jersey, 2001, P-1785, Monograph Number, p. 10074.
- [2] G. Ayhan-Kılıçgil, C. Kuş, E.D. Özdamar, B. Can-Eke, M. İşcan, Arch. Pharm. 340 (2007) 607–611.
- [3] C. Kuş, G. Ayhan-Kılıçgil, B. Can-Eke, M. İşcan, Arch. Pharm. Res. 27 (2004) 156–163.
- [4] Z. Ateş-Alagöz, C. Kuş, T. Çoban, J. Enzyme Inhib. Med. Chem. 20 (2005) 325–331.
- [5] G. Navarrete-Vázquez, R. Cedillo, A. Hernández-Campos, L. Yépez, F. Hernández-Luis, J. Valdez, R. Morales, R. Cortés, M. Hernández, R. Castillo, Bioorg. Med. Chem. Lett. 11 (2001) 187–190.
- [6] S.K. Katiyar, V.R. Gordon, G.L. McLaughlin, T.D. Edlind, Antimicrob. Agents Chemother. 38 (1994) 2086–2090.
- [7] E. Ravina, R. Sanchez-Alonso, J. Fueyo, M.P. Baltar, J. Bos, R. Iglesias, M.L. Sanmartin, Arzneim.-Forsch./Drug Res. 43 (1993) 689–694.
- [8] L. Garuti, M. Roberti, M. Malagoli, T. Rossi, M. Castelli, Bioorg. Med. Chem. Lett. 10 (2000) 2193–2195.
- [9] A. Rao, A. Chimirri, E. De Clercq, A.M. Monforte, P. Monforte, C. Pannecouque, M. Zappalá, Il Farmaco 57 (2002) 819–823.
- [10] A. Chimirri, A. De Sarro, G. De Sarro, R. Gitto, M. Zappalá, Il Farmaco 56 (2001) 821–826.
- [11] P.A. Thakurdesai, S.G. Wadodkar, C.T. Chopade, Pharmacologyonline 1 (2007) 314–329.
- [12] H.-T. Le, I.B. Lemaire, A.-K. Gilbert, F. Jolicœur, L. Yang, N. Leduc, S. Lemaire, J. Pharmacol. Exp. Ther. 30 (2004) 146–155.
- [13] B. Serafin, G. Borkowska, J. Głowczyk, I. Kowalska, S. Rump, Pol. J. Pharmacol. Pharm. 41 (1989) 89–96.
- [14] K. Kubo, Y. Inada, Y. Kohara, Y. Sugiura, M. Ojima, K. Itoh, Y. Furukawa, Y.K. Nishikawa, T. Naka, J. Med. Chem. 36 (1993) 1772–1784.
- [15] A. Abdel-monem Abdel-hafez, Arch. Pharm. Res. 30 (2007) 678–684.
- [16] S. Ram, D.S. Wise, L.L. Wotring, J.W. McCall, L.B. Townsend, J. Med. Chem. 35 (1992) 539–547.
- [17] A.Ts. Mavrova, P. Denkova, Y.A. Tsenov, K.K. Anichina, D.I. Vutchev, Bioorg. Med. Chem. 15 (2007) 6291–6297.
- [18] G. Ayhan-Kılıçgil, N. Altanlar, Il Farmaco 58 (2003) 1345–1350.
- [19] S. Özden, D. Atabey, S. Yıldız, H. Göker, Bioorg. Med. Chem. 13 (2005) 1587–1597.
- [20] N. Terzioğlu, R.M. van Rijn, R.A. Bakker, I.J.P. De Esch, R. Leurs, Bioorg. Med. Chem. Lett. 14 (2004) 5251–5256.
- [21] H. Küçükbay, R. Durmaz, E. Orhan, S. Günel, Il Farmaco 58 (2003) 431–437.
- [22] N.M. Agh-Atabay, B. Dülger, F. Gücin, Eur. J. Med. Chem. 38 (2003) 875–881.
- [23] M. Andrzejevska, L. Yépez-Mulia, R. Cedillo-Rivera, A. Tapia, L. Vilpo, J. Vilpo, Z. Kazimierzczuk, Eur. J. Med. Chem. 37 (2002) 973–978.
- [24] S.E. Castilo-Blum, N. Barba-Behrens, Coord. Chem. Rev. 196 (2003) 3–30.
- [25] K.K. Mothilal, C. Karunakaran, A. Rajendran, R. Murugesan, J. Inorg. Biochem. 98 (2004) 322–332.
- [26] J.B. Wright, Chem. Rev. 48 (1951) 397–541.
- [27] P.N. Preston, Chem. Rev. 74 (1974) 279–314.
- [28] X.-L. Zheng, Y. Liu, M. Pan, X.-Q. Lü, J.-Y. Zhang, C.-Y. Zhao, Y.-X. Tong, C.-Y. Su, Angew. Chem. Int. Ed. Engl. 46 (2007) 7399–7403.
- [29] D.-Q. Qi, G.-G. Hou, J.-P. Ma, R.-Q. Huang, Y.-B. Dong, Acta Crystallogr. C65 (2009) o85–o87.
- [30] W.A. Herrmann, Angew. Chem. Int. Ed. Engl. 41 (2002) 1290–1309.
- [31] S. Mohan, N. Sundaraganesan, J. Mink, Acta Part A 47 (1991) 1111–1115.
- [32] T.D. Klots, P. Devlin, W.B. Collier, Spectrochim. Acta Part A 53 (1997) 2445–2456.
- [33] M.A. Morsy, M.A. Al-Khaldi, A. Suwaiyan, J. Phys. Chem. A 106 (2002) 9196–9203.
- [34] Ş. Yurdakul, C. Yılmaz, Vib. Spectro. 21 (1999) 127–132.
- [35] A.W. Kleij, D.M. Tooke, A.L. Spek, J.N.H. Reek, Eur. J. Inorg. Chem. 22 (2005) 4626–4634.
- [36] G.M. Sheldrick, SHELXS-97 Program for the Solution of Crystal Structures, University of Göttingen, Germany, 1997.
- [37] L.J. Farrugia, J. Appl. Crystallogr. 32 (1999) 837–838.
- [38] G.M. Sheldrick, SHELXL-97 Program for Crystal Structures Refinement, University of Göttingen, Germany, 1997.
- [39] Stoe, Cie, X-Area Version 1.18 and X-RED32 Version 1.04, Stoe & Cie, Darmstadt, Germany, 2002.
- [40] A.L. Spek, Acta Crystallogr. D65 (2009) 148–155.
- [41] C. Peng, P.Y. Ayala, H.B. Schlegel, M.J. Frisch, J. Comput. Chem. 17 (1996) 49–56.
- [42] R. Dennington II, T. Keith, J. Millam, Gauss View, Version 4.1.2, Semicem Inc., Shawnee Mission, KS, 2007.
- [43] M.J. Frisch, G.W. Trucks, H.B. Schlegel, G.E. Scuseria, M.A. Robb, J.R. Cheeseman, J.A. Montgomery Jr., T. Vreven, K.N. Kudin, J.C. Burant, J.M. Millam, S.S. Iyengar, J. Tomasi, V. Barone, B. Mennucci, M. Cossi, G. Scalmani, N. Rega, G.A. Petersson, H. Nakatsuji, M. Hada, M. Ehara, K. Toyota, R. Fukuda, J. Hasegawa, M. Ishida, T. Nakajima, Y. Honda, O. Kitao, H. Nakai, M. Klene, X. Li, J.E. Knox, H.P. Hratchian, J.B. Cross, V. Bakken, C. Adamo, J. Jaramillo, R. Gomperts, R.E. Stratmann, O. Yazyev, A.J. Austin, R. Cammi, C. Pomelli, J.W. Ochterski, P.Y. Ayala, K. Morokuma, G.A. Voth, P. Salvador, J.J. Dannenberg, V.G. Zakrzewski, S. Dapprich, A.D. Daniels, M.C. Strain, O. Farkas, D.K. Malick, A.D. Rabuck, K. Raghavachari, J.B. Foresman, J.V. Ortiz, Q. Cui, A.G. Baboul, S. Clifford, J. Cioslowski, B.B. Stefanov, G. Liu, A. Liashenko, P. Piskorz, I. Komaromi, R.L. Martin, D.J. Fox, T. Keith, M.A. Al-Laham, C.Y. Peng, A. Nanayakkara, M. Challacombe, P.M.W. Gill, B. Johnson, W. Chen, M.W. Wong, C. Gonzalez, J.A. Pople, Gaussian 03, Revision E.01, Gaussian, Inc., Wallingford CT, 2004.
- [44] A.D. Becke, J. Chem. Phys. 98 (1993) 5648–5652.
- [45] C. Lee, W. Yang, R.G. Parr, Phys. Rev. B 37 (1988) 785–789.
- [46] R. Krishnan, J.S. Binkley, R. Seeger, J.A. Pople, J. Chem. Phys. 72 (1980) 650–654.
- [47] M.J. Frisch, J.A. Pople, J.S. Binkley, J. Chem. Phys. 80 (1984) 3265–3269.
- [48] P.M. Anbarasan, M.K. Subramanian, P. Senthilkumar, C. Mohanasundaram, V. Ilangovan, N. Sundaraganesan, J. Chem. Pharm. Res. 3 (2011) 597–612.
- [49] R. Ditchfield, J. Chem. Phys. 56 (1972) 5688–5691.
- [50] K. Wolinski, J.F. Hinton, P. Pulay, J. Am. Chem. Soc. 112 (1990) 8251–8260.
- [51] E. Cancès, B. Mennucci, J. Tomasi, J. Chem. Phys. 107 (1997) 3032–3041.
- [52] K. Brandenburg, DIAMOND Demonstration Version 3.2.f, Crystal Impact GbR, Bonn Germany, 2006.
- [53] O.Z. Yeşilel, M. Odabaşoğlu, O. Büyükgüngör, J. Mol. Struct. 874 (2008) 151–158.
- [54] E.B. Usova, E.Y. Kambulov, V.E. Zavadnik, G.D. Krapivin, Chem. Heterocycl. Comp. 35 (1999) 231–239.
- [55] T.-F. Tan, J. Han, M.-L. Pang, H.-B. Song, Y.-X. Ma, J.-B. Meng, Cryst. Growth Des. 6 (2006) 1186–1193.
- [56] Y.-S. Chen, K. Zhang, S.-Q. Zhao, Acta Crystallogr. E65 (2009) o1926.
- [57] F.H. Allen, O. Kennard, D.G. Watson, L. Brammer, A.G. Orpen, R. Taylor, J. Chem. Soc., Perkin Trans. II 12 (1987) S1–S19.
- [58] F.H. Allen, Acta Crystallogr. B58 (2002) 380–388.
- [59] I.J. Bruno, J.C. Cole, P.R. Edgington, M. Kessler, C.F. Macrae, P. McCabe, J. Pearson, R. Taylor, Acta Crystallogr. B58 (2002) 389–397.
- [60] J. Yin, R.L. Elsenbaumer, J. Org. Chem. 70 (2005) 9436–9446.
- [61] N. Sundaraganesan, S. Ilakiamani, P. Subramani, B.D. Joshua, Spectrochim. Acta A 67 (2007) 628–635.
- [62] P. Politzer, J.S. Murray, Theor. Chem. Acc. 108 (2002) 134–142.
- [63] F.J. Luque, J.M. Lopez, M. Orozco, Theor. Chem. Acc. 103 (2000) 343–345.
- [64] N. Okulik, A.H. Jubert, Internet Electron. J. Mol. Des. 4 (2005) 17–30.
- [65] P. Politzer, P.R. Laurence, K. Jayasuriya, Environ. Health Perspect. 61 (1985) 191–202.
- [66] P. Politzer, D.G. Truhlar, Chemical Applications of Atomic and Molecular Electrostatic Potentials, Plenum, New York, 1981.
- [67] I. Fleming, Frontier Orbitals and Organic Chemical Reactions, Wiley, London, 1976.
- [68] Y.-X. Sun, Q.-L. Hao, W.-X. Wei, Z.-X. Yu, L.-D. Lu, X. Wang, Y.-S. Wang, J. Mol. Struct. THEOCHEM 904 (2009) 74–82.
- [69] V.M. Geskin, C. Lambert, J.-L. Brédas, J. Am. Chem. Soc. 125 (2003) 15651–15658.
- [70] D. Sajan, H. Joe, V.S. Jayakumar, J. Zaleski, J. Mol. Struct. 785 (2006) 43–53.
- [71] G.A. Babu, P. Ramasamy, Curr. Appl. Phys. 10 (2010) 214–220.